Heliyon 9 (2023) e22737

Contents lists available at ScienceDirect

Heliyon

journal homepage: www.cell.com/heliyon

Dual solutions of unsteady flow of copper-alumina/water based hybrid nanofluid with acute magnetic force and slip condition

Ghulam Rasool [a,b,*], Wang Xinhua [a,**], Liaquat Ali Lund [c], Ubaidullah Yashkun [d], Abderrahim Wakif [e], Adnan Asghar [c]

[a] Institute of Intelligent Machinery, Faculty of Materials and Manufacturing, Beijing University of Technology, Beijing, 100124, China
[b] Department of Mechanical Engineering, Lebanese American University, Beirut, Lebanon
[c] School of Quantitative Sciences, Universiti Utara Malaysia, 06010, Sintok, Kedah, Malaysia
[d] Department of Mathematics and Social Sciences, Sukkur IBA University, Sukkur, Pakistan
[e] Laboratory of Mechanics, Faculty of Sciences Aïn Chock, Hassan II University, Casablanca, Morocco

ARTICLE INFO

Keywords:
Hybrid nanofluid (HN)
Duality
Slip condition
Acute magnetic field
Stability analysis

ABSTRACT

Suspending particles of tiny solid in a fluid used to transport energy can enhance its thermal conductivity and heat transport properties. Our main goal of this examination is to study the radiative unsteady two-dimensional (2D) flow on a continuously diminishing, horizontal sheet. with suction for the hybrid water-based nanofluid and an aligned field of magnetic, including the combined suction, magnetic, and velocity slip conditions effect. The Tiwari & Das model of nanofluid equations is used, which takes into consideration the solid volume percentage. Equations of similarity are derived by employing the transformations of similarity, and the associated equations have been simplified numerically by employing the bvp4c method in MATLAB software for a variety of values of the nanoparticle volume fraction, the unsteadiness, and the wall mass suction in water. It is discovered that, within the given the unsteadiness parameter range, two solutions exist. Moreover, it is found that the fluid velocity slows down in 1st solution as volume fraction of copper nanoparticles rises but speeds up in the second solution at first before slowing down again. Using a temporal stability analysis, it is found that only one of the dual branches is stable over the long run, while the other is unstable.

1. Introduction

Increasing global energy demands include irreversible energy sources such as energy storage, fossil fuels, and thermal resource heat exchangers. The development of natural resources has devastating environmental consequences, such as worldwide heating and air pollution. To fill in these gaps, researchers and experts have concentrated on improving production of renewable energy processes, such as generation of solar energy. The cheapest and cleanest renewable energy resource is solar energy, that can be turned into thermal which is ecologically friendly. In the form of heat-changing fluids and solar collectors, these types of energy may be

* Corresponding author. Institute of Intelligent Machinery, Faculty of Materials and Manufacturing, Beijing University of Technology, Beijing, 100124, China.
** Corresponding author. Institute of Intelligent Machinery, Faculty of Materials and Manufacturing, Beijing University of Technology, Beijing, 100124, China.
E-mail addresses: grasool@bjut.edu.cn (G. Rasool), sunxhking@aliyun.com (W. Xinhua).

https://doi.org/10.1016/j.heliyon.2023.e22737
Received 18 June 2023; Received in revised form 16 November 2023; Accepted 17 November 2023
Available online 22 November 2023

Nomenclature

β	Acute angle
nf	Nanofluid properties
ρ_{nf}	Nanofluid effective density (Kgm^{-3})
T_w	Sheet variable temperature (K)
M	Hartmann/magnetic number
$(c_p)_{hnf}$	HN heat capacitance (JK^{-1})
σ	Electrical conductivity (Sm^{-1})
σ_1	Stefan–Boltzmann constant
T_0	A constant
Rd	Thermal radiation
T_∞	Ambient temperature (K)
$(c_p)_{nf}$	Nanofluid heat capacitance (JK^{-1})
f	Fluid fraction
u, v	Velocity components (ms^{-1})
N_u	Nusselt number
ρ_{hnf}	HN effective density (Kgm^{-3})
S	$S>0$ for blowing and $S<0$ for suction
μ_{hnf}	HN effective dynamic viscosity
$'$	Differentiation with respect to η
hnf	HN properties
μ_{nf}	Nanofluid effective dynamic viscosity
A^*	Initial velocity slip factor
B_0	Constant applied magnetic field
C_f	Skin friction coefficient
Re	Local Reynolds number
k_{hnf}	HN thermal conductivity $(Wm^{-1}K^{-1})$
k_{nf}	Nanofluid thermal conductivity $(Wm^{-1}K^{-1})$
v_w	Suction/injection velocity (ms^{-1})
k^*	Mean absorption coefficient
$\varphi_{Al_2O_3}$	Alumina nanoparticle volume fraction
c	Constant
t	Time (s)
T	Temperature (K)
B	Magnetic field
A	Unsteadiness parameter
Pr	Prandtl number
φ_{Cu}	Copper nanoparticle volume fraction
γ	Smallest eigen value
δ	Velocity slip
η	Transformed variable
τ	Stability transformed variable

discovered. The collectors absorb solar photons via a permeable sheet and transfer the heat to an absorbent solution (e.g., water mixture, water). However, given that they demonstrate poor thermal competence during the modification process, their lower thermal capacity is their most obvious shortcoming. One initiative to increase the thermal efficiency of technology in recent years has received an inordinate amount of attention: switching from conventional running fluids to nanofluids.

Particles in nanofluids range in size from 1 to 100 nm, and their dispersion is stable [1]. Numerous different physical processes, such as energy storage make extensive use of nanofluids [2]. Mebarek-Oudina [3] analyzed the nanofluids flow utilizing various base fluids. Sheikholeslami et al. [4] reported an exhaustive nanofluid flow numerical simulation including viscous dissipation and magnetic effects. Li et al. [5] considered the flow of nanofluid inside a permeable duct employing the Buongiorno model for external power due to the good usage of nano liquid. Reddy et al. [6] inspected the effects of magnetic-hydrodynamics (MHD) water-based nano--liquids mixing in a spinning disk within a permeable channel on the chemically reactive heat trade-off dynamics. Recent years have seen a lot of thermal environment research and energy fields using numerical and analytical approaches for nano-fluids and heat transfer. For example, according to Khan et al. [7] & Zaim et al. [8], they created hybrid nanofluid by mixing binary kinds of nanoparticles that are introduced to traditional fluids and can be applied in several heat exchange applications. Khan et al. [9,10]

constructed and studied the transient flow of $(Cu - Al_2O_3/H_2O)$, and found that the inclusion of 5 % nanomaterials significantly enhanced the Nusselt number performance. Hayat & Nadeem [11] explored the instigation of energy transfer via the expanding sheet of $(Cu - Ag/H_2O)$, hybrid nanofluids. Sundar et al. [12] investigated the resistance property and energy transfer phenomena of $(MWCNT - Fe_3O_4/H_2O)$ hybrid nanofluid. Sohail et al. [13] analyzed the mobility of nanofluid in three dimensions in a flexible media when heat radiation was present. Along with the research publications, the following contemporary works might be quoted to learn more about the hybrid nanofluid procedure in different geometries [14–18]. Roy et al. [19] studied the heat transfer of dusty hybrid nanofluid flow over an unsteady shrinking sheet in the presence of a magnetic field. They discovered that an increase in the magnetic field parameter, the suction parameter, and the mixture density ratio results in an increase in the skin friction coefficient and the local Nusselt number. An effective investigation on nanofluid using thermal radiation and MHD as well as the flow and heat transfer of a second-grade hybrid nanofluid is over a permeable stretching/shrinking sheet also in Refs. [20–22].

It is significant to remember that magnetohydrodynamics is one of the elements that stimulates fluid mechanics, or MHD, property. These phenomena are represented by electroconductive fluid flow in the presence of field of magnetic. The influence of MHD in the physical, industrial, and engineering areas has a staggering number of ramifications. Examples include generators of MHD power, granular insulation, MHD flow meters, device sterilization, magnetic resonance imaging, material sealing, sink-float separation, and loudspeaker construction [23–24]. Tian et al. [25]'s computer investigation of magnetohydrodynamics boundary layer flow revealed that flow of fluid had been significantly impacted by field of magnetic and that the convective method for heat transfer had been impeded. Rahman et al. [26] demonstrated the effect of Brownian motion and thermophoresis on stagnation point at oblique of nanofluid flow. They noticed that when the thermophoresis parameter increases, the temperature differential between the solid surface and ambient fluid increases, while parameter of the Brownian motion increases flow of convective. Numerous scholars [27–34] are now examining the MHD flow in different geometries. There are other studies on the flow of hydromagnetic viscous fluid, Cattaneo-Christov heat flux in nonlinear radiative hybrid mass diffusion, and Cattaneo-Christov heat flux in three-phase oscillatory flow on non-Newtonian fluid see Refs. [35–39]. The industrial world can benefit from the current model. The Tiwari and Das nanofluid model is employed to investigate different geometries, nanoparticles, and their physical properties, such as viscosity, thermal conductivity, and heat capacity, as well as the role of cavities in the creation of entropy.

The primary objective of this study is to investigate the 2D time dependent flow of aligned MHD of a hybrid nanofluid over a contracting sheet by incorporating the effects of radiation and velocity slip condition. The considered hybrid nanofluid is conductive electrically, controlled by a magnetic field oriented at an acute angle β, and is produced by incorporating $Cu - Al_2O_3$ nanoparticles into the base liquid (H_2O). According to the authors' knowledge and information, the present research is original and has not been previously explored, as shown by a careful examination of previously published works. In addition, the current problem's innovations may be identified via the provision of dual solutions accompanied by an investigation of the stability of the solutions. This study provides answers to the questions regarding its extensive applications in diverse manufacturing and engineering procedures. (i) How do the volume percentage of solid particles and suction parameters affect the coefficient of skin friction and heat transfer rate? (ii) How the rate of heat transfer improves when $Cu - Al_2O_3$ nanoparticles are added to water (H_2O) as the base fluid. (iii) What impact does the inclination angle of the field of magnetic have on velocity profiles and the skin friction coefficient? (iv) Where do stable and unstable solutions converge, and what makes them different? Similar patterns of applicable and relevant research questions have been provided by Shah et al. [40] and Sowmya et al. [41] for the problem under consideration. The goal of this work is to improve the thermal conductivity and heat transfer of fundamental fluids by introducing acute magnetic force and slip situation. This study demonstrates that adding microscopic particles to basic fluids can improve heat transfer efficiency, which is something that researchers have been working to do in the literature.

2. Problem formulation

This study considers the thermal radiation impact on the incompressible, unsteady flow of $Cu - Al_2O_3$/water hybrid nanofluid along a shrinking surface. The model of problem in system of coordinate is presented in Fig. 1. The fluid is conductive and is affected by a magnetic field that is aligned randomly at an acute angle (β) of $B = \frac{B_0}{\sqrt{(1-\varepsilon t)}}$, where B_0 is the constant applied magnetic field. Wall mass

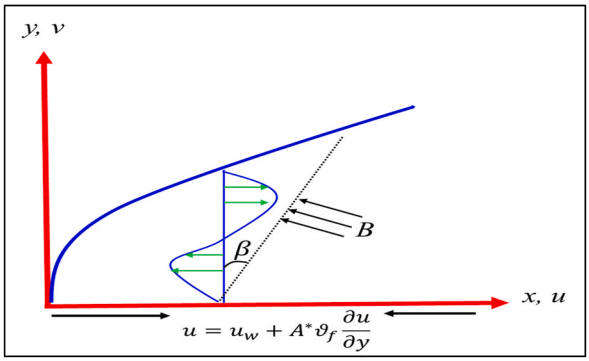

Fig. 1. Model of the problem and coordinate systems.

transfer velocity is given by $v_w(x) = -\left(\frac{\vartheta c}{(1-\varepsilon t)}\right)^{\frac{1}{2}} S$, where c is a positive constant. The Tiwari and Das [42] mathematical nanofluid model is used in this instance. The governing equations for this study are derived from the laws of conservation of mass, momentum, and energy. In the presence of magnetic force and slip condition, the governing boundary layer equations for continuity, momentum, and thermal energy are provided as following equations (1)–(4):

$$\frac{\partial u}{\partial x}+\frac{\partial v}{\partial y}=0 \tag{1}$$

$$\frac{\partial u}{\partial t}+u\frac{\partial u}{\partial x}+v\frac{\partial u}{\partial y}=\frac{\mu_{hnf}}{\rho_{hnf}}\frac{\partial^2 u}{\partial y^2}-\frac{\sigma_{hnf}B^2}{\rho_{hnf}}\sin^2\beta u \tag{2}$$

$$\frac{\partial T}{\partial t}+u\frac{\partial T}{\partial x}+v\frac{\partial T}{\partial y}=\left[\frac{k_{hnf}}{(\rho c_p)_{hnf}}+\frac{16\sigma_1 T_\infty^3}{3k^*(\rho c_p)_{hnf}}\right]\frac{\partial^2 T}{\partial y^2} \tag{3}$$

Following are the boundary conditions for the specified problem:

$$\begin{cases} t<0, u=v=0, T=T_\infty \\ t\geq 0, v=v_w, u=u_w+A^*\vartheta_f\dfrac{\partial u}{\partial y}, T=T_w \text{at } y=0 \\ u\to 0, T\to T_\infty \text{as } y\to\infty \end{cases} \tag{4}$$

The surface velocity is given by $u_w(x,t) = = -\frac{cx}{(1-\varepsilon t)}$. In this investigation, we shall use Waini et al. [43]'s approach to thermophoresis. The characteristics of the hybrid nanofluids are listed in Tables 1–2.

The following similarity variables will be used further to turn the governing equations into a system of ordinary differential equations (ODEs).

$$\eta=\left(\frac{c}{\vartheta(1-\varepsilon t)}\right)^{\frac{1}{2}} y, u=\frac{cx}{(1-\varepsilon t)}f'(\eta), v=-\left(\frac{\vartheta c}{(1-\varepsilon t)}\right)^{\frac{1}{2}} f(\eta), \theta(\eta)=\frac{T-T_\infty}{T_w-T_\infty} \tag{5}$$

By putting Equation (5) into Equations (1)–(3), Equation (1) is unquestionably satisfied, and Equations (2) and (3) reduced into the corresponding ODEs (6–8).

$$\frac{\mu_{hnf}/\mu_f}{\rho_{hnf}/\rho_f}f''' + ff'' - f'^2 - A(0.5\eta f'' + f') - \frac{\sigma_{hnf}/\sigma_f}{\rho_{hnf}/\rho_f}M\sin^2\beta f' = 0 \tag{6}$$

$$\frac{1}{Pr(\rho c_p)_{hnf}/(\rho c_p)_f}\left[(k_{hnf}/k_f)+\frac{4Rd}{3}\right]\theta'' + f\theta' - 0.5A\eta\theta' = 0 \tag{7}$$

Along with BCs

$$\begin{cases} f(0)=S, f'(0)=-1+\delta f''(0), \theta(0)=1 \\ f'(\eta)\to 0, \theta(\eta)\to 0 \text{as} \eta\to\infty \end{cases} \tag{8}$$

The reduced quantities are stated as follows: $A=\frac{\varepsilon}{c}, \delta=A^*\sqrt{c\vartheta_f}, M=\frac{\sigma_f B_0^2}{c\rho_f}, Pr=\frac{\vartheta_f}{\alpha_f}, Rd=\frac{4\sigma_1 T_\infty^3}{k^* k_f}$ where A is the unsteadiness parameter, δ is the first order velocity slip, M is the magnetic parameter, Pr is the Prandtl number, and Rd is the thermal radiation parameter.

Table 1
Hybrid nanofluid properties of thermophysical [43].

Properties	Hybrid Nanofluid
Dynamic viscosity	$\mu_{hnf}/\mu_f = \frac{1}{(1-\varphi_{Cu})^{2.5}(1-\varphi_{Al_2O_3})^{2.5}}$
Density	$\rho_{hnf}/\rho_f = (1-\varphi_{Al_2O_3})[(1-\varphi_{Cu})+\varphi_{Cu}\rho_{Cu}/\rho_f]+\varphi_{Al_2O_3}\rho_{Al_2O_3}/\rho_f$
Electrical conductivity	$\sigma_{hnf}=\frac{\sigma_{Cu}+2\sigma_{nf}-2\varphi_{Cu}(\sigma_{nf}-\sigma_{Cu})}{\sigma_{Cu}+2\sigma_{nf}+\varphi_{Cu}(\sigma_{nf}-\sigma_{Cu})}\times(\sigma_{nf})$ where $\sigma_{nf}=\frac{\sigma_{Al_2O_3}+2\sigma_f-2\varphi_{Al_2O_3}(\sigma_f-\sigma_{Al_2O_3})}{\sigma_{Al_2O_3}+2\sigma_f+\varphi_{Al_2O_3}(\sigma_f-\sigma_{Al_2O_3})}\times(\sigma_f)$
Thermal conductivity	$k_{hnf}=\frac{k_{Al_2O_3}+2k_{nf}-2\varphi_{Al_2O_3}(k_{nf}-k_{Al_2O_3})}{k_{Al_2O_3}+2k_{nf}+\varphi_{Al_2O_3}(k_{nf}-k_{Al_2O_3})}\times(k_{nf})$ where $k_{nf}=\frac{k_{Cu}+2k_f-2\varphi_{Cu}(k_f-k_{Cu})}{k_{Cu}+2k_f+\varphi_{Cu}(k_f-k_{Cu})}\times(k_f)$
Heat capacity	$(\rho c_p)_{hnf}/(\rho c_p)_f = (1-\varphi_{Al_2O_3})[(1-\varphi_{Cu})+\varphi_{Cu}(\rho c_p)_{Cu}/(\rho c_p)_f]+\varphi_{Al_2O_3}(\rho c_p)_{Al_2O_3}/(\rho c_p)_f$

Table 2
The properties of thermos physical [43].

Properties	Water (H_2O)	Copper (Cu)	Alumina (Al_2O_3)
$\rho\,(kg/m^3)$	997.1	8933	3970
$c_p(J/kg\,K)$	4179	385	765
$k\,(W/m\,K)$	0.613	400	40
$\sigma(S/m)$	0.05	5.96×10^7	3.69×10^7
Pr	6.2		

The physical quantities of attention are the skin friction coefficient C_f and local Nusselt number Nu_x, these are expressed as

$$C_f=\frac{\mu_{hnf}}{\rho_f u_w^2}\left(\frac{\partial u}{\partial y}\right)|y=0, Nu_x=-\frac{xk_{hnf}}{k_f(T_w-T_\infty)}\left(\frac{\partial T}{\partial y}\right)|y=0 \tag{9}$$

By applying Equation (5) in Equation (9), we have equation (10):

$$\sqrt{Re}C_f=\frac{1}{\left(1-\varphi_{Al_2O_3}\right)^{2.5}(1-\varphi_{Cu})^{2.5}}f''(0); \sqrt{\frac{1}{Re}}Nu_x=-\frac{k_{hnf}}{k_f}\left[1+\frac{4Rd}{3}\right]\theta'(0) \tag{10}$$

where Re is local Reynold number.

3. Stability analysis

It is necessary to include the new time-dependent dimensionless similarity variable by considering $\tau=\frac{ct}{(1-\varepsilon t)}$ in order to do the temporal analysis of solutions stability, as recommended by Merkin [44] & Dero et al. [45,46].

$$\begin{cases} u=\dfrac{cx}{(1-\varepsilon t)}\dfrac{\partial f(\eta,\tau)}{\partial\eta}, v=-\left(\dfrac{\vartheta c}{(1-\varepsilon t)}\right)^{\frac{1}{2}}f(\eta,\tau), \theta(\eta,\tau)=\dfrac{T-T_\infty}{T_w-T_\infty} \\ \eta=\left(\dfrac{c}{\vartheta(1-\varepsilon t)}\right)^{\frac{1}{2}}y; \tau=\dfrac{ct}{(1-\varepsilon t)} \end{cases} \tag{11}$$

Putting Equation (11) in place of Equations (2) and (3) yields equations 13 and 14 as follows:

$$\frac{\mu_{hnf}/\mu_f}{\rho_{hnf}/\rho_f}\frac{\partial^3 f}{\partial\eta^3}+f\frac{\partial^2 f}{\partial\eta^2}-\left(\frac{\partial f}{\partial\eta}\right)^2-A\left(0.5\eta\frac{\partial^2 f}{\partial\eta^2}+\frac{\partial f}{\partial\eta}\right)-(1+A\tau)\frac{\partial^2 f}{\partial\tau\partial\eta}-\frac{\sigma_{hnf}/\sigma_f}{\rho_{hnf}/\rho_f}M\sin^2\beta f'=0 \tag{12}$$

$$\frac{1}{Pr(\rho c_p)_{hnf}/(\rho c_p)_f}\left[(k_{hnf}/k_f)+\frac{4Rd}{3}\right]\frac{\partial^2\theta}{\partial\eta^2}+f\frac{\partial\theta}{\partial\eta}-0.5A\eta\frac{\partial\theta}{\partial\eta}-(1+A\tau)\frac{\partial\theta}{\partial\tau}=0 \tag{13}$$

Subject to BCs

$$\begin{cases} f(0,\tau)=S, \dfrac{\partial f(0,\tau)}{\partial\eta}=-1+\delta\dfrac{\partial^2 f(0,\tau)}{\partial\eta^2}, \theta(0,\tau)=1 \\ \dfrac{\partial f\eta(,\tau)}{\partial\eta}=\theta(\eta,\tau)=0\ as\ \eta\to\infty \end{cases} \tag{14}$$

To evaluate the solutions for steady flow, stability where $f(\eta)=f_0(\eta)$, and$\theta(\eta)=\theta_0(\eta)$ satisfying the boundary value problem (6–8) is as equation (15):

$$\begin{cases} f(\eta,\tau)=f_0(\eta)+e^{-\gamma\tau}F(\eta,\tau) \\ \theta(\eta,\tau)=\theta_0(\eta)+e^{-\gamma\tau}G(\eta,\tau) \end{cases} \tag{15}$$

where $G(\eta)$ and $F(\eta)$ are small relative of $\theta_0(\eta)$ and $f_0(\eta)$, and γ is the parameter for the eigenvalues that has not yet been determined. To obtain the linearized eigenvalue problem, substituted Equation (15) into Equations (12) and (13) with $\tau=0$, yields equations 16–18:

$$\frac{\mu_{hnf}/\mu_f}{\rho_{hnf}/\rho_f}F_0'''+f_0F_0''-2f_0'F_0'+F_0f_0''-A\left(0.5\eta F_0''+F_0'\right)+\gamma F_0'-\frac{\sigma_{hnf}/\sigma_f}{\rho_{hnf}/\rho_f}M\sin^2\beta F_0'=0 \tag{16}$$

$$\frac{1}{Pr(\rho c_p)_{hnf}/(\rho c_p)_f}\left[(k_{hnf}/k_f)+\frac{4Rd}{3}\right]G_0''+f_0G_0'+F_0\theta_0'-0.5\eta AG_0'+\gamma G_0=0 \tag{17}$$

Subject to BCs

$$\begin{cases} F_0(0)=0, F_0'(0)=\delta F_0''(0), G_0(0)=0 \\ F_0'(\eta)\to 0, G_0(\eta)\to 0 \ as \ \eta\to\infty \end{cases} \tag{18}$$

For the smallest eigenvalues to be obtained, one boundary condition must be loosened/relaxed, as stated by Khashi'ie et al. [47] and Haris et al. [48]. This relaxing of the boundary conditions has no discernible effect on the outcomes [49]. For this problem, we changed $F_0'(\eta)\to 0 as \eta\to\infty$ into $F_0''(0)=1$.

4. Algorithm of numerical method (bvp4c)

The following steps are a brief outline of the steps involved in using the *bvp4c* method in MATLAB.

1. Define $f\left(x, y, \frac{dy}{dx}\right)$ as a differential equation.
2. Define the $y(a)$ and $y(b)$ boundary conditions.
3. Developed a function (in MATLAB) to represent the discretized system of ODEs.
4. To initialize the solution guess for the ODE solver, use the **bvpinit** function.
5. To solve the BVP, use the **bvp4c** function.
6. As input arguments to **bvp4c**, pass the differential equation function, boundary condition function, and initial guess from step 4.
7. To solve the system of ODEs and obtain the numerical solution to the BVP, **bvp4c** internally employs an ODE solver.
8. Obtain the solution from the **bvp4c** output.

5. Result and discussion

In current section of the article, the numerical *bvp4c* technique implemented in MATLAB to converse the numerical outcomes of present MHD unsteady flow of hybrid nanofluid along with the effect of velocity slip, suction, and thermal radiation over the shrinking sheet. The resulting ODEs (06–07) of the problem connected to BCs are as follows (08). The method is elaborately outlined by Shampine et al. [50]. Many plots use the solid volume fraction $\varphi_{Al_2O_3}=0.1$, as suggested by Devi & Devi [51]. To complete the $Cu-Al_2O_3$/water hybrid nanofluid, added the solid volume fractions φ_{Cu}. Prandtl number $Pr=6.2$ is used throughout this study as a fixed parameter, per the advice of Iqbal et al. [52] and Dero et al. [53]. As a means of assessing the efficacy of the procedure, Fig. 2 is displayed for evaluation. Results show that the critical points from the present research agree well with those from the literature (see graph six of Waini et al. [54]). Currently this approach will be effective in solving this problem after comparing it to others.

The temperature and velocity curves for φ_{Cu} are shown in Figs. 3 and 4, respectively. It is found that the fluid velocity drops in the first solution as φ_{Cu} rises, although it increases in the second solution at first and later decreases. Specifically, the velocity profile is lowered by increasing the volume percentage, which is a result of the creation of entropy and heat transport in both kinds of moving fluids. However, it appears that as the copper nanoparticles percentage $\varnothing_{Cu}$ grows, the hybrid nanofluid temperature also rises (see Fig. 4).

For different values of S, the velocity $f'(\eta)$ profiles and temperature $\theta(\eta)$ profiles have been portrayed in Figs. 5 and 6. Increases in the suction parameter S reduce fluid velocity in first solution. Suction improves the flow near the wall's surface by decreasing the thickness of the momentum boundary layer, which may be a physical explanation for this effect. However, it is known that suction reduces the initial solution's temperature. When the suction parameter S is raised, the fluid velocity in the lower branch rises and the fluid temperature falls.

Fig. 7 displays the changes in velocity $f'(\eta)$ profiles caused by varying the velocity slip parameter δ. For larger values of δ, both solutions of $f'(\eta)$ exhibit a reduction in the velocity field and the thickness of the momentum boundary layer, which, in practice,

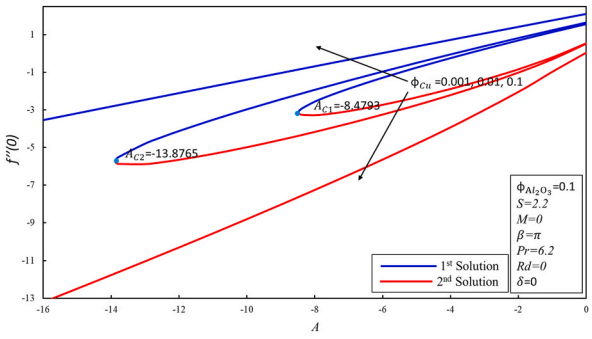

Fig. 2. The contrast to Waini et al. [45]'s Fig. 6.

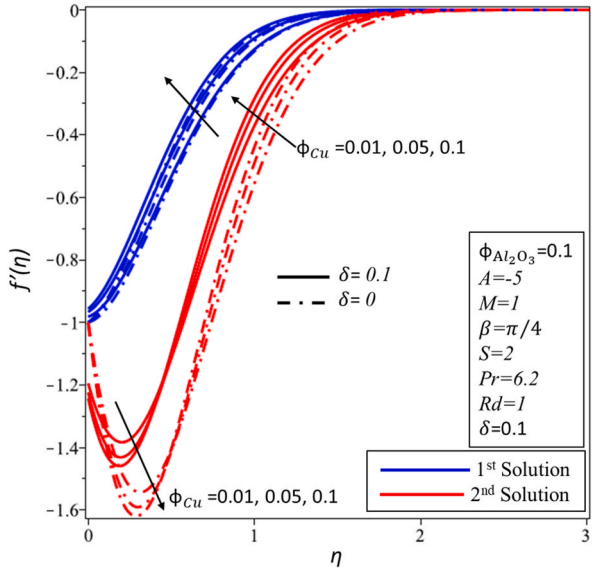

Fig. 3. $f'(\eta)$ changes as function of η for various φ_{Cu} values.

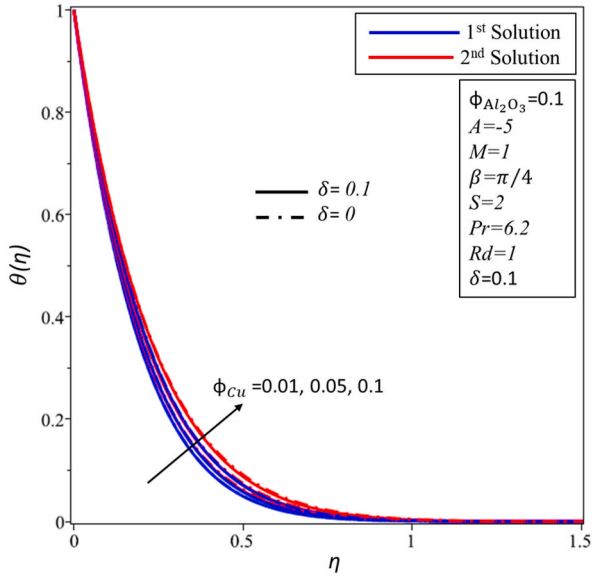

Fig. 4. $\theta(\eta)$ changes as function of η for various φ_{Cu} values.

demonstrates that the viscosity of hybrid nanofluid rises in this region of boundary layer.

Fig. 8 illustrates the impact of thermal radiation parameter *Rd* over, temperature profiles $\theta(\eta)$. The thickness of thermal layer and fluid temperature rise with higher *Rd* values. Because of the increased thermal state of the surroundings caused by radiation heat, the thermal transfer is placed on the moving hybrid nanofluid, which in turn increases the thermal conductivity to barriers of radiation. Therefore, temperature and thermal boundary layer thickness increase in both solutions.

For the values of $\varphi_{Cu} = 0.001, 0.01$, and 0.1, the plots in Figs. 9 and 10 depict the evolution of $f''(0)$ and $-\theta'(0)$ against unsteadiness parameter *A*, respectively. These figures show, as in Fang et al. [55], that "there are regions of unique solution and regions with more than one solution (dual solutions)", where the identical values of $A(<0)$ give rise to two different solutions for the same φ_{Cu}. For all values of *A*, there is only one solution when *A* is equal to a critical number $A_c(<0)$, and no solutions exist when *A* is less than A_c. Thus, solutions are possible up to the critical values A_c, after which the boundary disconnects from the surface and solutions based on the boundary estimates are no longer feasible.

Figs. 11 and 12 depict the evolution of $f''(0)$ and $-\theta'(0)$ along *M* for a wide range of φ_{Cu}. The critical point of *M* is seen to increase in value along with the solid volume percentage φ_{Cu}. Furthermore, for φ_{Cu}= 0.001 and 0.01, the corresponding critical values of *M* are

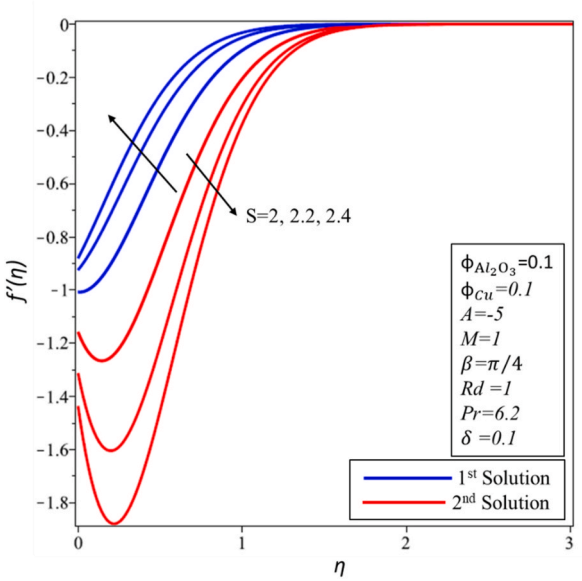

Fig. 5. $f'(\eta)$ changes as function of η for different S values.

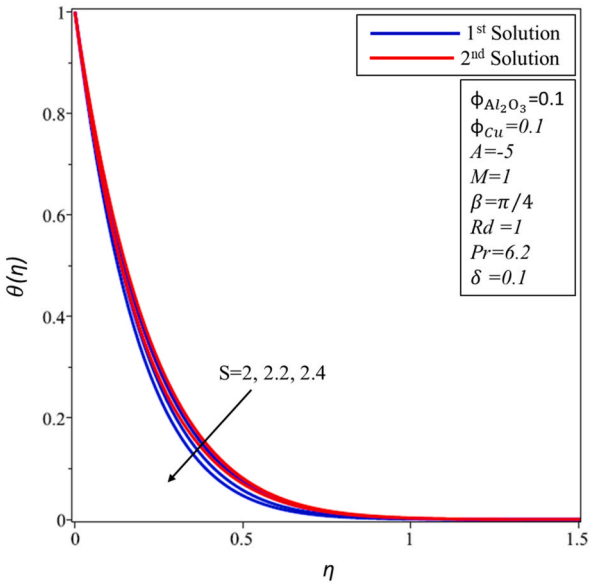

Fig. 6. $\theta(\eta)$ changes as function of η for various S values.

$M_{c1} = 0.4500, M_{c2} = 0.4001$. The physical reason for the boundary layer separation's thickening is examined and find that the critical points of M reduce with rising values of solid volume percentage φ_{Cu}. Furthermore, it can be noted that increasing the solid volume fraction φ_{Cu} increases the magnitudes of $f''(0)$ in the initial solution while decreasing them in the second solution. Furthermore, as φ_{Cu} rises, the unstable and stable solution experiences a decrease in heat transfer. The critical values of the parameter M decreases due to increasing of the values φ_{cu}.At positive values of M the critical values of M_{c3} is negligible at $\varphi_{cu} = 0.1$.

The findings of this study shows that the values of the least eigenvalue (γ) can be found in Table 03. A negative score clearly shows that the disturbance is escalating, as can be seen in the table, while a positive value of indicates that the flow is stabilizing. In addition, for the critical values of A for both solutions, it is seen that γ goes to zero.

6. Conclusion

In this study, magnetic and slip conditions effect is investigated along with the unsteady flow of a hybrid copper-alumina/water

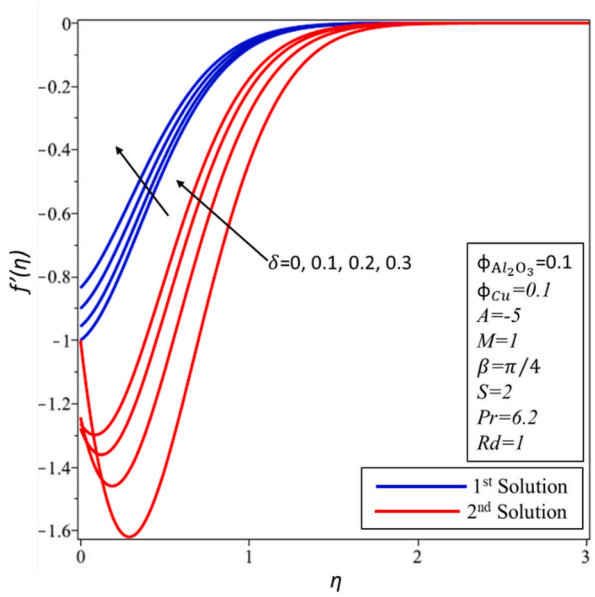

Fig. 7. $f'(\eta)$ changes as function of η for various δ values.

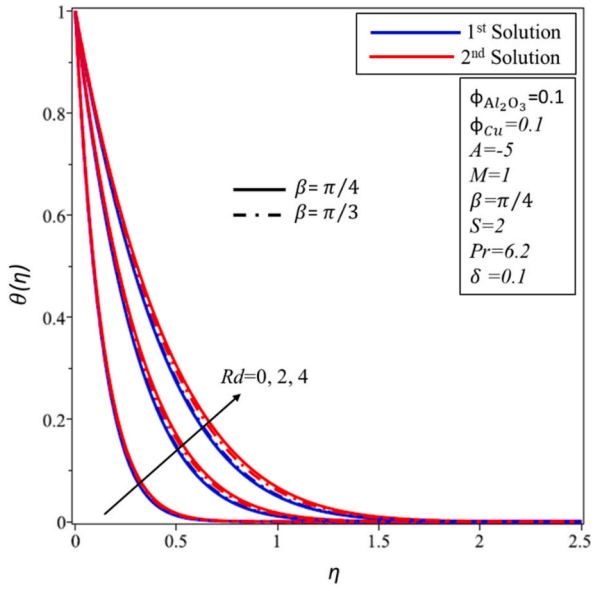

Fig. 8. $\theta(\eta)$ changes as function of η for various Rd values.

based nanofluid. The governing ODEs for the flow and heat transport are solved using the BVP4C technique in MATLAB software. The obtained results are compared graphically with the earlier results presented by Waini et al. [54] and found a good agreement. Nanoparticles with a Prandtl value of 6.2 (water) were used to study the unsteadiness $A(<0)$, the mass suction $S(>0)$, and the solid volume fraction factors effects on the flow and heat transfer. Our research shows that these parameters have a major effect on the heat transfer and flow. For a select set of parameters, dual solutions exist. When comparing heat transfer rate and skin friction coefficient, the two solutions are more apparent in the former. The region of dual solution for hybrid nanofluids expands as the volume fraction parameter rises. The volume fraction parameter has a significant impact on the temperature profiles, but they are not notably sensitive to the different types of nanoparticles. Only the first solution is stable, while the second one is shown to be unstable by the stability analysis.

It is found that for increasing the values of solid volume fraction the critical values of M reduce. Numerical results exhibit that the hybrid nanofluid gains a higher heat transfer rate than the pure fluid. In future more accurate results can get by adding acute magnetic force and slip condition in hybrid nanofluids.

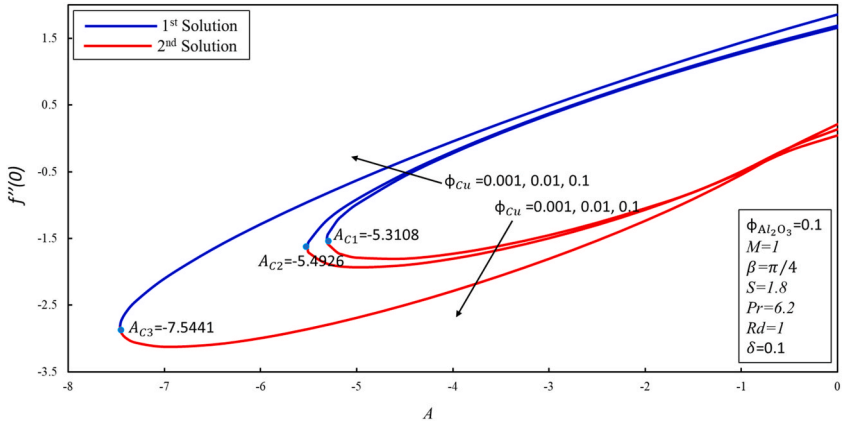

Fig. 9. The relationship between A and the value of $f''(0)$ at different values of φ_{Cu}.

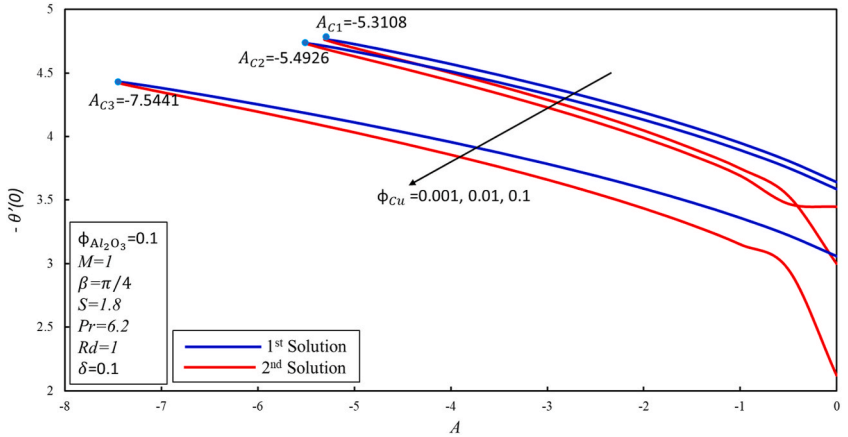

Fig. 10. The relationship between A and the value of $-\theta'(0)$ at different values of φ_{Cu}.

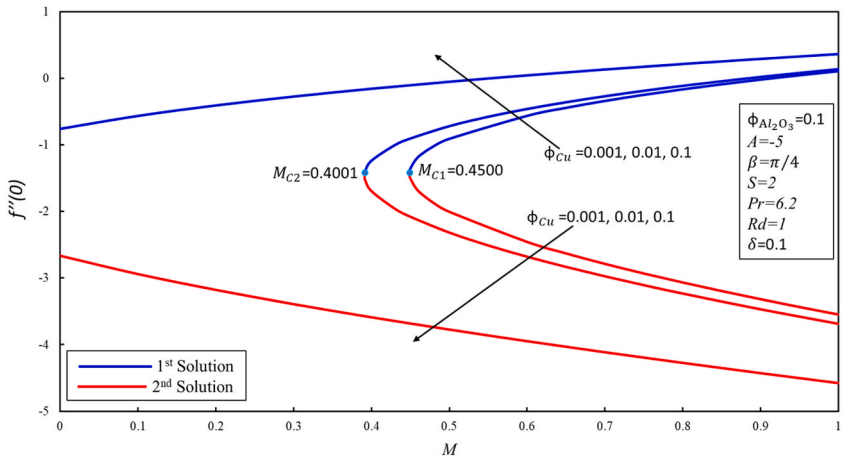

Fig. 11. The relationship between M and the value of $f''(0)$ at different values of φ_{Cu}.

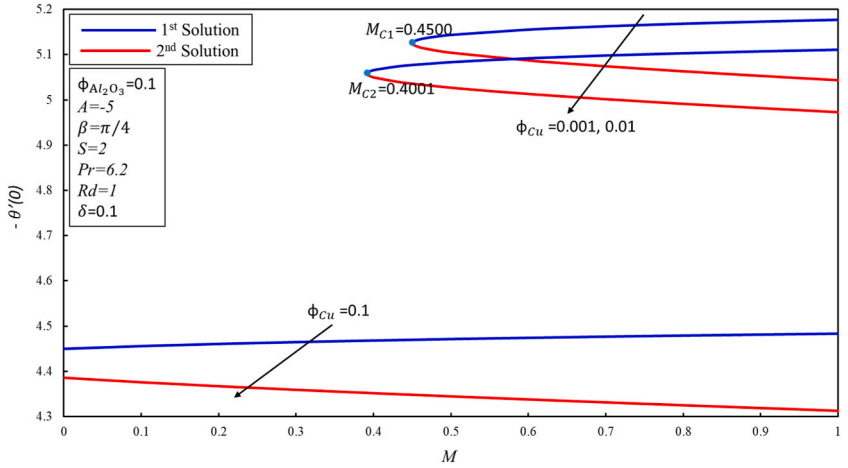

Fig. 12. The relationship between M and the value of $-\theta'(0)$ at different values of φ_{Cu}.

Table 3
Smallest eigen values γ at various estimates of A and $\varnothing_{Cu}$ as $\varnothing_{Al_2O_3} = 0.1, M = 1, \beta = \frac{\pi}{4}, S = 1.8, Pr = 6.2, Rd = 1,$ and $= 0.1$.

$\varnothing_{Cu}$	A	γ	
		1st solution	2nd solution
0.001	−4.5	0.4962	−0.46328
	−5	0.3662	−0.26382
	−5.3108	0.000	0.000
0.01	−4.5	0.6096	−0.7362
	−5	0.4502	−0.3683
	−5.4926	0.000	0.000
0.1	−5	0.8136	−0.8964
	−6	0.5009	−0.6601
	−7.5441	0.000	0.000

Data availability statement

No data was used for the research described in the article.

Funding

The first author is thankful to the National Foreign Expert Project-Foreign Youth Talent Program Fund No. QN2023001001, Beijing Natural Science Foundation Project- Foreign Scholar Program Fund No. IS23046, Beijing Postdoctoral Research Activities Fund No. Q6001A00202301 for supporting this research.

CRediT authorship contribution statement

Ghulam Rasool: Conceptualization, Formal analysis, Funding acquisition, Investigation, Project administration, Resources, Supervision, Visualization, Writing – original draft, Writing – review & editing. **Wang Xinhua:** Formal analysis, Project administration, Supervision, Visualization, Writing – original draft, Writing – review & editing. **Liaquat Ali Lund:** Conceptualization, Data curation, Formal analysis, Investigation, Software, Validation, Writing – original draft, Writing – review & editing. **Ubaidullah Yashkun:** Conceptualization, Data curation, Formal analysis, Methodology, Writing – original draft, Writing – review & editing. **Abderrahim Wakif:** Conceptualization, Data curation, Formal analysis, Validation, Visualization, Writing – original draft, Writing – review & editing. **Adnan Asghar:** Formal analysis, Validation, Visualization, Writing – original draft, Writing – review & editing.

Declaration of competing interest

The authors declare that they have no known competing financial interests or personal relationships that could have appeared to influence the work reported in this paper.

References

[1] S.U. Choi, J.A. Eastman, *Enhancing Thermal Conductivity of Fluids with Nanoparticles* (No. ANL/MSD/CP-84938; CONF-951135-29), Argonne National Lab.(ANL), Argonne, IL (United States), 1995.
[2] T. Gul, W. Noman, M. Sohail, M.A. Khan, Impact of the Marangoni and thermal radiation convection on the graphene-oxide-water-based and ethylene-glycol-based nanofluids, Adv. Mech. Eng. 11 (6) (2019) 1–9.
[3] F. Mebarek-Oudina, Convective heat transfer of Titania nanofluids of different base fluids in cylindrical annulus with discrete heat source, Heat Tran. Asian Res. 48 (1) (2019) 135–147.
[4] M. Sheikholeslami, S. Abelman, D.D. Ganji, Numerical simulation of MHD nanofluid flow and heat transfer considering viscous dissipation, Int. J. Heat Mass Tran. 79 (2014) 212–222.
[5] Z. Li, S. Saleem, A. Shafee, A.J. Chamkha, S. Du, Analytical investigation of nanoparticle migration in a duct considering thermal radiation, J. Therm. Anal. Calorim. 135 (3) (2019) 1629–1641.
[6] P.S. Reddy, P. Sreedevi, A.J. Chamkha, MHD boundary layer flow, heat and mass transfer analysis over a rotating disk through porous medium saturated by Cu-water and Ag-water nanofluid with chemical reaction, Powder Technol. 307 (2017) 46–55.
[7] O. Toker, H. Ozbay, On the NP-hardness of solving bilinear matrix inequalities and simultaneous stabilization with static output feedback, in: Proceedings of 1995 American Control Conference-Acc'95, vol. 4, IEEE, 1995, June, pp. 2525–2526.
[8] A. Zaim, A. Aissa, F. Mebarek-Oudina, B. Mahanthesh, G. Lorenzini, M. Sahnoun, M. El Ganaoui, Galerkin finite element analysis of magneto-hydrodynamic natural convection of Cu-water nanoliquid in a baffled U-shaped enclosure, Propulsion and Power Research 9 (4) (2020) 383–393.
[9] U. Khan, M. Asadullah, N. Ahmed, S.T. Mohyud-Din, Influence of Joule heating and viscous dissipation on MHD flow and heat transfer of viscous fluid in converging/diverging stretchable channels, Journal of Nanofluids 6 (2) (2017) 254–263.
[10] U. Khan, N. Ahmed, S.T. Mohyud-Din, Surface thermal investigation in water functionalized nanomaterials-based nanofluid over a sensor surface, Appl. Nanosci. (2020) 1–11.
[11] T. Hayat, S. Nadeem, Heat transfer enhancement with Ag–CuO/water hybrid nanofluid, Results Phys. 7 (2017) 2317–2324.
[12] L.S. Sundar, M.K. Singh, A.C. Sousa, Enhanced heat transfer and friction factor of MWCNT–Fe3O4/water hybrid nanofluids, Int. Commun. Heat Mass Tran. 52 (2014) 73–83.
[13] M. Sohail, R. Naz, S.I. Abdelsalam, On the onset of entropy generation for a nanofluid with thermal radiation and gyrotactic microorganisms through 3D flows, Phys. Scripta 95 (4) (2020), 045206.
[14] M.G. Reddy, N. Kumar, B.C. Prasannakumara, N.G. Rudraswamy, K.G. Kumar, Magnetohydrodynamic flow and heat transfer of a hybrid nanofluid over a rotating disk by considering Arrhenius energy, Commun. Theor. Phys. 73 (4) (2021), 045002.
[15] H. Waqas, S.M.R.S. Naqvi, M.S. Alqarni, T. Muhammad, Thermal transport in magnetized flow of hybrid nanofluids over a vertical stretching cylinder, Case Stud. Therm. Eng. 27 (2021), 101219.
[16] M. Gholinia, M.E. Hoseini, S. Gholinia, A numerical investigation of free convection MHD flow of Walters-B nanofluid over an inclined stretching sheet under the impact of Joule heating, Therm. Sci. Eng. Prog. 11 (2019) 272–282.
[17] A.S. Sabu, A. Wakif, S. Areekara, A. Mathew, N.A. Shah, Significance of nanoparticles' shape and thermo-hydrodynamic slip constraints on MHD alumina-water nanoliquid flows over a rotating heated disk: the passive control approach, Int. Commun. Heat Mass Tran. 129 (2021), 105711.
[18] U. Khan, A. Shafiq, A. Zaib, A. Wakif, D. Baleanu, Numerical exploration of MHD falkner-skan-sutterby nanofluid flow by utilizing an advanced non-homogeneous two-phase nanofluid model and non-fourier heat-flux theory, Alex. Eng. J. 59 (6) (2020) 4851–4864.
[19] N.C. Roy, A. Hossain, I. Pop, Flow and heat transfer of MHD dusty hybrid nanofluids over a shrinking sheet, Chin. J. Phys. 77 (2022) 1342–1356.
[20] N.C. Roy, I. Pop, Dual solutions of a nanofluid flow past a convectively heated nonlinearly shrinking sheet, Chin. J. Phys. 82 (2023) 31–40.
[21] N.C. Roy, P. Pop Ioan, Unsteady magnetohydrodynamic stagnation point flow of a nanofluid past a permeable shrinking sheet, Chin. J. Phys. 75 (2022) 109–119.
[22] N.C. Roy, I. Pop, Flow and heat transfer of a second-grade hybrid nanofluid over a permeable stretching/shrinking sheet, Eur. Phys. J. A 135 (2020) 768.
[23] S.A. Shehzad, Z. Abdullah, A. Alsaedi, F.M. Abbasi, T. Hayat, Thermally radiative three-dimensional flow of Jeffrey nanofluid with internal heat generation and magnetic field, J. Magn. Magn Mater. 397 (2016) 108–114.
[24] Y.S. Daniel, Z.A. Aziz, Z. Ismail, F. Salah, Double stratification effects on unsteady electrical MHD mixed convection flow of nanofluid with viscous dissipation and Joule heating, J. Appl. Res. Technol. 15 (5) (2017) 464–476.
[25] X.Y. Tian, B.W. Li, J.K. Zhang, The effects of radiation optical properties on the unsteady 2D boundary layer MHD flow and heat transfer over a stretching plate, Int. J. Heat Mass Tran. 105 (2017) 109–123.
[26] M.M. Rahman, T. Grosan, I. Pop, Oblique stagnation-point flow of a nanofluid past a shrinking sheet, Int. J. Numer. Methods Heat Fluid Flow 26 (1) (2016) 189–213.
[27] W.H. Huang, A. Abidi, M.R. Khan, D. Jing, E.E. Mahmoud, F.M. Allehiany, A.M. Galal, Numerical Study of Heat Transfer and Friction Drag in MHD Viscous Flow of a Nanofluid Subject to the Curved Surface, Waves in Random and Complex Media, 2021, pp. 1–16.
[28] R. Ali, M.R. Khan, A. Abidi, S. Rasheed, A.M. Galal, Application of PEST and PEHF in magneto-Williamson nanofluid depending on the suction/injection, Case Stud. Therm. Eng. 27 (2021), 101329.
[29] M.R. Khan, A. Abidi, J. Madiouli, K. Guedri, A.M. Al-Bugami, T.H. Al-arabi, A.M. Galal, Impact of Joule heating and viscous dissipation on magnetohydrodynamics boundary layer flow of viscous nanofluid subject to the stretched surface, Proc. IME E J. Process Mech. Eng. (2021), 09544089211064120.
[30] A. Jamaludin, K. Naganthran, R. Nazar, I. Pop, MHD mixed convection stagnation-point flow of Cu-Al2O3/water hybrid nanofluid over a permeable stretching/shrinking surface with heat source/sink, Eur. J. Mech. B Fluid 84 (2020) 71–80.
[31] S. Nadeem, A.U. Khan, MHD oblique stagnation point flow of nanofluid over an oscillatory stretching/shrinking sheet: existence of dual solutions, Phys. Scripta 94 (7) (2019), 075204.
[32] X. Li, A.U. Khan, M.R. Khan, S. Nadeem, S.U. Khan, Oblique stagnation point flow of nanofluids over stretching/shrinking sheet with Cattaneo–Christov heat flux model: existence of dual solution, Symmetry 11 (9) (2019) 1070.
[33] A. Rashid, M. Ayaz, S. Islam, A. Saeed, P. Kumam, P. Suttiarporn, Theoretical analysis of the MHD flow of a tangent hyperbolic hybrid nanofluid over a stretching sheet with convective conditions: a nonlinear thermal radiation case, S. Afr. J. Chem. Eng. 42 (2022) 255–269.
[34] M.M. Rahman, A.J. Chamkha, Y. Elmasry, I. Ullah, A.A. Pasha, M.S. Sadeghi, A.M. Galal, The heat transfer behavior of MHD micro-polar MWCNT-Fe3O4/Water Hybrid Nano-fluid in an inclined⊥ shaped cavity with semi-circular heat source inside, Case Stud. Therm. Eng. 38 (2022), 102316.
[35] M. Naveed, Z. Abbas, M. Sajid, et al., Dual solutions in hydromagnetic viscous fluid flow past a shrinking curved surface, Arabian J. Sci. Eng. 43 (2018) 1189–1194.
[36] Z. Abbas, A. Rehman, S. Khaliq, M.Y. Rafiq, Flow dynamics of MHD hybrid nanofluid past a moving thin needle with a temporal stability test: a Galerkin method approach. Numerical Heat Transfer, Part B: Fundamentals 84 (3) (2023) 329–347.
[37] T. Rahim, J. Hasnain, N. Abid, Z. Abbas, Entropy generation for mixed convection flow in vertical annulus with two regions hydromagnetic viscous and Cu-Ag water hybrid nanofluid through porous zone: a comparative numerical study, Propulsion and Power Research 11 (3) (2022) 401–415.
[38] N. Fatima, J. Hasnain, N. Sanaullah Abid, M.M.A. Lashin, S.M. Eldin, Aspects of Cattaneo-Christov heat flux in nonlinear radiative ternary, hybrid, and single mass diffusion past stretching surface; A comparative study, Case Stud. Therm. Eng. 43 (2023), 102776.
[39] J. Hasnain, N. Abid, M.O. Alansari, M. Zaka Ullah, Analysis on Cattaneo-Christov heat flux in three-phase oscillatory flow of non-Newtonian fluid through porous zone bounded by hybrid nanofluids, Case Stud. Therm. Eng. 35 (2022), 102074.
[40] N.A. Shah, I.L. Animasaun, J.D. Chung, A. Wakif, F.I. Alao, C.S.K. Raju, Significance of nanoparticle's radius, heat flux due to concentration gradient, and mass flux due to temperature gradient: the case of Water conveying copper nanoparticles, Sci. Rep. 11 (1) (2021) 1–11.

[41] G. Sowmya, B.J. Gireesha, I.L. Animasaun, N.A. Shah, Significance of buoyancy and Lorentz forces on water-conveying iron (III) oxide and silver nanoparticles in a rectangular cavity mounted with two heated fins: heat transfer analysis, J. Therm. Anal. Calorim. 144 (6) (2021) 2369–2384.
[42] R.K. Tiwari, M.K. Das, Heat transfer augmentation in a two-sided lid-driven differentially heated square cavity utilizing nanofluids, Int. J. Heat Mass Tran. 50 (9–10) (2007) 2002–2018.
[43] I. Waini, A. Ishak, I. Pop, Hybrid nanofluid flow and heat transfer past a vertical thin needle with prescribed surface heat flux, Int. J. Numer. Methods Heat Fluid Flow 29 (2019), https://doi.org/10.1108/HFF-04-2019-0277.
[44] J.H. Merkin, On dual solutions occurring in mixed convection in a porous medium, J. Eng. Math. 20 (2) (1986) 171–179.
[45] S. Dero, M.J. Uddin, A.M. Rohni, Stefan blowing and slip effects on unsteady nanofluid transport past a shrinking sheet: multiple solutions, Heat Tran. Asian Res. 48 (2019), https://doi.org/10.1002/htj.21470.
[46] S. Dero, A.M. Rohni, A. Saaban, I. Khan, Dual solutions and stability analysis of micropolar nanofluid flow with slip effect on stretching/shrinking surfaces, Energies 12 (23) (2019) 4529.
[47] N.S. Khashi'ie, N.M. Arifin, M.M. Rashidi, E.H. Hafidzuddin, N. Wahi, Magnetohydrodynamics (MHD) stagnation point flow past a shrinking/stretching surface with double stratification effect in a porous medium, J. Therm. Anal. Calorim. (2019) 1–14.
[48] S.D. Harris, D.B. Ingham, I. Pop, Mixed convection boundary-layer flow near the stagnation point on a vertical surface in a porous medium: brinkman model with slip, Transport Porous Media 77 (2) (2009) 267–285.
[49] I. Waini, A. Ishak, I. Pop, Transpiration effects on hybrid nanofluid flow and heat transfer over a stretching/shrinking sheet with uniform shear flow, Alex. Eng. J. 59 (2020). https://doi.org/10.1016/j.aej.2019.12.010.
[50] L.F. Shampine, L.F. Shampine, I. Gladwell, S. Thompson, Solving ODEs with Matlab, Cambridge university press, 2003.
[51] S.A. Devi, S.S.U. Devi, Numerical investigation of hydromagnetic hybrid Cu–Al2O3/water nanofluid flow over a permeable stretching sheet with suction, Int. J. Nonlinear Sci. Numer. Stimul. 17 (5) (2016) 249–257.
[52] Z. Iqbal, N.S. Akbar, E. Azhar, E.N. Maraj, Performance of hybrid nanofluid (Cu-CuO/water) on MHD rotating transport in oscillating vertical channel inspired by Hall current and thermal radiation, Alex. Eng. J. 57 (3) (2018) 1943–1954.
[53] S. Dero, A.M. Rohni, A. Saaban, The dual solutions and stability analysis of nanofluid flow using tiwari-das modelover a permeable exponentially shrinking surface with partial slip conditions, J. Eng. Appl. Sci. 14 (2019) 4569–4582.
[54] I. Waini, A. Ishak, I. Pop, Unsteady flow and heat transfer past a stretching/shrinking sheet in a hybrid nanofluid, Int. J. Heat Mass Tran. 136 (2019) 288–297.
[55] F. Tie-Gang, Z. Ji, Y. Shan-Shan, Viscous flow over an unsteady shrinking sheet with mass transfer, Chin. Phys. Lett. 26 (1) (2009), 014703.